◆ Human Brain Mapping 39:532–541 (2018) ◆

Diffuse Brain Damage in Normal Tension Glaucoma

Antonio Giorgio,* Jian Zhang, Francesco Costantino, Nicola De Stefano ,† and Paolo Frezzotti†

Department of Medicine, Surgery and Neuroscience, University of Siena, Italy

Abstract: Brain changes within and beyond the visual system have been demonstrated in primary open angle glaucoma (POAG), the most common type of glaucoma. These changes have been often interpreted as a neurodegenerative process due, at least partially, to the raised intraocular pressure (IOP). In this context, normal tension glaucoma (NTG), a form of POAG with IOP <21 mm Hg despite the typical glaucomatous findings, represents the most suitable model of glaucoma to test the validity of this hypothesis. We acquired multimodal brain MRI in NTG patients ($n = 17$) and compared them with demographically matched groups of POAG patients with raised IOP ($n = 17$) and normal controls (NC, $n = 29$). Voxelwise statistics was performed with nonparametric permutation testing.

Both NTG and POAG patients showed, compared to NC, significantly more gray matter atrophy in both the visual system and in nonvisual brain regions and altered diffusion tensor imaging-derived anatomical connectivity (AC; lower fractional anisotropy and/or higher diffusivities). Compared with NTG, POAG had both more atrophic visual cortex and higher axial diffusivity in nonvisual regions. Functional connectivity (FC) with respect to NC was altered in NTG at short-range level [visual network (VN), ventral attention network] and in POAG at long-range level (between secondary VN and limbic network). FC of POAG was higher than NTG in both VN and executive network.

This study provides further evidence that diffuse structural and functional abnormalities across glaucoma brain may be, at least partially, independent of raised IOP and the consequent retinal degeneration. This further defines glaucoma as a condition with neurodegeneration spreading. *Hum Brain Mapp 39:532–541, 2018*.

Key words: glaucoma; MRI; connectivity; neurodegeneration; resting state networks; Alzheimer disease

INTRODUCTION

Primary open angle glaucoma (POAG) is one of the most important causes of irreversible blindness in the Caucasian population, with 2% prevalence in people older than 40 years. Normal tension glaucoma (NTG) is a form of POAG in which there is no clinical evidence of elevated intraocular pressure (IOP) but the presence of the typical glaucomatous findings [i.e., damage to the optic nerve head (ONH), progressive thinning of retinal nerve fiber layer (RNFL) and peculiar visual field (VF) defects] [Mallick et al., 2016].

NTG itself is less frequent than the classical POAG, also known as high-tension glaucoma (HTG), but its prevalence seems to vary in different populations. In fact, NTG cases represent about 25–32% of overall POAG cases, both in the Beaver Dam study in Wisconsin, USA [Klein et al., 1992] and in the Egna Neumarkt study in Alto Adige, Italy

†These authors contributed equally to the manuscript
*Correspondence to: Antonio Giorgio, MD PhD, Department of Medicine, Surgery and Neuroscience, University of Siena, Viale Bracci 2, 53100 Siena, Italy. E-mail: giorgio3@unisi.it

Received for publication 20 May 2017; Revised 6 October 2017; Accepted 16 October 2017.

DOI: 10.1002/hbm.23862

Published online 24 October 2017 in Wiley Online Library (wileyonlinelibrary.com).

TABLE I. Clinical-demographic characteristics of the NTG and POAG groups

Clinical-demographic characteristics	NTG patients ($n = 17$)	POAG patients ($n = 17$)	P-value
Age, mean ± SD (years)	58,9 ± 13,7	58,6 ± 13,4	$P = 0.95$, N.S.[a]
Sex, male/female	13/4	9/8	$P = 0.22$, N.S.[a]
GSS stage			$P = 0.99$, NS
Mild (n)	10	10	
Moderate (n)	2	2	
Severe (n)	5	5	
Type of the poorer performing eye (n)	Right (9), left (8)	Right (9), left (8)	$P = 0.99$, N.S.
IOP[b] (on treatment), mean ± SD (mm Hg)	14 ± 3.4	17.7 ± 4.2	$P = 0.007$
MD[b], mean ± SD (dB)	−8.28 ± 8.31	−9.99 ± 8.93	$P = 0.42$, N.S.
PSD[b], mean ± SD (dB)	6.52 ± 4.89	7 ± 3.54	$P = 0.36$, N.S.
RNFL[b], mean ± SD (μm)	74.35 ± 11.85	67.25 ± 16.35	$P = 0.17$, N.S.
Fazekas scale			$P = 0.79$, N.S.[c]
Grade 0	70.6%	58.8%	
Grade 1	17.7%	23.6%	
Grade 2	11.7%	17.6%	
Grade 3	None	None	

[a]Three-group comparison including NC.
[b]Poorer performing eye.
[c]Three-group comparison including NC ($n = 29$), in whom Fazekas scale was grade 0 (69%), grade 1 (27.5%), grade 2 (3.5%), and none in grade 3.
See text for abbreviations.

[Bonomi et al., 1998] whereas NTG prevalence is three to four times higher than HTG in Japan [Shiose et al., 1991]. In POAG with raised IOP, we and others have previously demonstrated through multimodal brain MRI widespread damage of diffusion tensor imaging (DTI)-derived anatomical connectivity (AC), gray matter (GM) atrophy and/or altered resting state functional connectivity (FC) that can go beyond the visual system, even since the early disease stage [Dai et al., 2013; Frezzotti et al., 2014, 2016; Jiang et al., 2017; Wang et al., 2016, 2017; Zikou et al., 2012].

The possible occurrence of WM hyperintensities (WMH) in the brain of POAG patients may be the expression of small vessel vascular changes and thus an additional risk factor for POAG pathogenesis and/or the consequence of neuronal degeneration [Schoemann et al., 2014]. However, WMH can be present in the general population, increasing with aging [Pantoni and Garcia, 1997].

Overall, the studies of advanced MRI in POAG have questioned whether retinal degeneration is the unique neuropathological process underpinning glaucoma and whether raised IOP can play a main role in determining widespread brain abnormalities. For this reason, NTG would represent the most suitable model to test whether or not widespread neurodegeneration across brain may occur independently of raised IOP. To the best of our knowledge, evidence of MRI-derived brain abnormalities in NTG is currently limited. An MRI study on the anterior visual pathway of NTG showed reduced volumetry and altered DTI measures, which correlated with RNFL thickness and VF measures [Zhang et al., 2012]. A more recent DTI study in NTG patients from Japan, where the disease has a high prevalence, found decreased fractional anisotropy (FA) compared with normal controls (NC) in the occipital WM comprising optic radiations (OR) and forceps major (F_{maj}) but also in nonvisual areas such as corpus callosum (CC) and parietal lobe [Boucard et al., 2016].

The aims of this study were to assess whether (i) in NTG, in absence of the raised IOP occurring in the classical POAG, there is evidence of neurodegenerative findings in both visual system and in other systems across brain; (ii) the presence of raised IOP, as in patients with classical POAG, may represent a worsening factor for brain abnormalities in comparison with NTG.

MATERIAL AND METHODS

Study Subjects and Ophthalmological Evaluation

We recruited 34 POAG patients whose clinical and demographic characteristics are summarized in Table I. The patients were defined as affected by glaucoma if they fulfilled the following criteria: typical glaucomatous VF loss on either Octopus or Humphrey perimetry and glaucomatous alterations of the ONH [Iester et al., 1997]. Based on the IOP values the POAG patient population was divided into two groups: HTG-POAG (POAG hereafter, $n = 17$) if IOP ≥21 mm Hg and NTG ($n = 17$) if IOP <21 mm Hg.

Data were also compared with those of 29 NC (age = 57.9 ± 9.9 years, 15 male).

All patients were recruited among those who were consecutively referring to the Glaucoma Service of the

University of Siena and each patient underwent a complete ophthalmologic evaluation: anterior segment examination, central corneal ultrasonic pachymetry (OcuScan RxP; Alcon Laboratories, Irvine, CA), uncorrected and best corrected visual acuity, gonioscopy with grading according to the Van Hericke ShafferseSchwartz grading system [Van Herick et al., 1969], fundus examination, IOP measurement with Goldmann tonometer (six times a day in order to rule out the presence of diurnal IOP spikes), VF examination and RNFL thickness. VF were recorded, as previously described [Frezzotti et al., 2014, 2016] using the Humphrey Field Analyser (Carl Zeiss Meditec, Dublin, CA) running the 30-2 program SITA-Standard, which provided VF indices such as: (i) mean deviation (MD), which is the average deviation of sensitivity at each test location from age-adjusted normal population values, representing an indication of the degree of the generalized loss in the VF; (ii) pattern standard deviation (PSD), which is a summary measure of the average deviation of individual VF. Peripapillary RNFL thickness was measured using the Optic Disc Cube 200 × 200 scanning protocol of the Cirrus OCT (Carl Zeiss Meditec, Dublin, CA), as previously described [Frezzotti et al., 2016]. Glaucoma patients were classified with Hodapp/Bascom Palmer glaucoma severity staging system (GSS) [Hodapp et al., 1993]. All patients required treatment to both eyes to reduce IOP. Exclusion criteria were age > 80 years, any ocular disorder other than glaucoma, any neurological disorder (documented clinically and instrumentally), the presence of significant cerebrovascular condition on MRI (i.e., WMH of grade 3 on the Fazekas scale) [Fazekas et al., 1987] or WMH fulfilling the MRI criteria for multiple sclerosis [Polman et al., 2011] or radiologically isolated syndrome [Okuda et al., 2009], and use of medications that can affect the VF.

Subjects in the NC group were recruited among laboratory and hospital workers, had normal neurological and ophthalmological examinations and no history of neurological or ophthalmological disorders.

The study received approval from the local Ethics Committee (Azienda Ospedaliera Universitaria Senese). Informed written consent was obtained from all subjects before study entry.

MRI Acquisition

In all subjects brain MRI was acquired at the NMR Center of the University of Siena on a 1.5 Tesla Philips Gyroscan (Philips Medical Systems, Best, The Netherlands). A sagittal survey image was used to identify the anterior and posterior commissures. Sequences were acquired in the axial plane parallel to the commissural line. A FLAIR image [repetition time (TR) = 9,000 ms, echo time (TE) = 150 ms, inversion recovery delay = 2,725 ms, voxel size = 1 × 1 × 3 mm] was acquired for WMH assessment. DTI data consisted of echo-planar imaging (EPI) (TR = 8,500 ms; TE = 100 ms; voxel size = 2.5 mm^3), with diffusion weighting distributed in 32 directions and *b*-value = 1,000 $s*mm^{-2}$. The resting-fMRI data were 190 volumes of EPI sequence with TR = 1,000 ms, TE = 50 ms, voxel size = 3.75 × 3.75 × 6 mm. A high-resolution T1-weighted image (TR = 25 ms, TE = 4.6 ms, voxel size = 1 mm^3) was acquired for image registration, anatomical mapping and analysis of GM volume.

MRI Analysis

It was performed at the Quantitative Neuroimaging Laboratory of the University of Siena

White matter hyperintensities

A single observer with longstanding MRI experience (A.G.) visually assessed FLAIR images. The grading of WMH was visually assessed with Fazekas scale. In addition, the WMH volume was computed after outlining their borders with a semiautomated segmentation technique based on user-supervised local thresholding (Jim 5.0; Xinapse System; www. xinapse.com/Manual/)

Voxelwise analysis of DTI images

DTI data were firstly preprocessed with DTIPrep (www.nitrc.org/projects/dtiprep/) [Oguz et al., 2014], a tool for automatic quality control which minimizes various types of artifacts. Then, we used FDT (FMRIB Diffusion Toolbox), part of FSL (FMRIB Software Library, www.fmrib.ox.ac.uk/fsl/) [Jenkinson et al., 2012; Smith et al., 2004] to obtain, by fitting a diffusion tensor model, images of FA, axial diffusivity (AD), and radial diffusivity (RD).The subsequent analysis was performed with TBSS (Tract-Based Spatial Statistics), which registered DTI images into a common standard space (FMRIB58_FA) using FNIRT non linear registration and created, from the mean FA images, the mean WM "skeleton" (thresholded at FA > 0.2), representing the centers of all tracts common to the whole study population, onto which registered DTI images were finally projected

Voxelwise analysis GM volumes

It was performed on 3D T1-weighted images with FSL-voxel based morphometry (VBM) [Douaud et al., 2007], which uses an optimized VBM protocol [Good et al., 2001], according to a previously used procedure [Frezzotti et al., 2014, 2016; Giorgio et al., 2015]. Briefly, T1-W images were brain-extracted, GM-segmented, and registered onto the MNI152 standard space using FNIRT. Then, all native GM images were nonlinearly registered onto a symmetric study-specific GM template, modulated and smoothed (isotropic Gaussian kernel, sigma = 3 mm).

Voxelwise analysis of resting FMRI

For each subject, several preprocessing steps were performed on resting FMRI image: removal of the first five volumes to allow signal stability; initial motion correction by volume-realignment to the middle volume using MCFLIRT (FMRIB's Linear Image Registration Tool) [Jenkinson and Smith, 2001]; nonbrain removal using BET; global 4D mean intensity normalization; spatial smoothing (6 mm full width at half maximum); registration to the T1-weighted image using affine boundary-based registration cost as implemented in FLIRT [Jenkinson and Smith, 2001], and subsequent transformation to MNI152 standard space using nonlinear registration FNIRT (warp resolution: 10 mm); use of ICA-AROMA [independent component analysis (ICA)-based automatic removal of motion artifacts, https://github.com/rhr-pruim/ICA-AROMA] to further remove motion-related artifacts [Pruim et al., 2015]; regression of WM and cerebrospinal fluid (CSF; both thresholded at a very conservative threshold of 95% tissue probability) to remove residual structured noise; application of a high-pass temporal filtering (cut-off frequency of 100 s); final normalization to MNI152 standard space using FNIRT. The filtered, normalized FMRI images of all study subjects were concatenated across time into a single 4D image, which was then automatically decomposed by MELODIC [Multivariate Exploratory Linear Optimized Decomposition into Independent Components (ICs), http://fsl.fmrib.ox.ac.uk/fsl/fslwiki/MELODIC] [Beckmann and Smith, 2004; Beckmann et al., 2005] into a set of 13 ICs, a number which was automatically estimated using the Laplace approximation to the Bayesian evidence of the model order. ICs of interest were selected by visual inspection and by comparison with previously described resting state networks (RSNs) [Smith et al., 2009] and reflect "coactivation" or "synchronization" across the network. One IC represented physiological noise (CSF pulsations) and was thus discarded before further processing.

Finally, voxelwise intranetwork (short-range) FC analysis was performed using the "dual-regression" approach, where the set of spatial maps from the group-average analysis was used to generate subject-specific versions of the spatial maps and associated timeseries [Beckmann et al., 2009]. The outputs of the first-stage dual regression, that is, the subject-specific timeseries, were used for estimating temporal correlation between all the pairs of the RSNs, which is a measure of internetwork (or long-range) FC strength, using FSLNets (http://fsl.fmrib.ox.ac.uk/fsl/fslwiki/FSLNets). All internetwork Pearson r correlation coefficients were transformed into z-scores using the Fisher transform to improve data normality and then clustered hierarchically for each of the three group comparisons, thus leading to different functional groupings of the RSNs. Full correlation allows for the influence of other networks on RSN pairs while partial correlation represents a more direct relationship between RSN pairs.

Statistics

As for general statistics, the differences among the three groups were tested with analysis of variance (ANOVA) for age and log-transformed WMH volume and with Chi-square for sex and WMH grade. Differences in opthalmological measures (MD, PSD, RNFL) between the two patient groups were assessed with Mann-Whitney test. Data were considered significant at $P < 0.05$. SPSS was used to perform such statistical analyses.

As for voxelwise analysis, group differences in DTI measures, GM volumes and RSN-FC were performed in the general linear model framework with ANOVA (i.e., F-test followed by post-hoc pairwise comparisons of NTG, POMS, and NC) using "randomize," a nonparametric permutation testing ($n = 5{,}000$) [Winkler et al., 2014]. Thresholding of statistical images was performed with Threshold-Free Cluster Enhancement, with a significance level of $P \leq 0.005$, uncorrected for multiple comparisons across space and with cluster size ≥ 30 voxels. Subsequently, following an approach using by other studies [Anjari et al., 2007; Frezzotti et al., 2014, 2016] to further confirm our results we computed in each subject mean values across voxels of significant clusters from between-group comparisons and applied ANOVA, using Bonferroni correction for multiple comparisons. Age and sex were set as covariates in all the analyses. WM and GM regions corresponding to local maxima within significant clusters were anatomically mapped using standard-space atlases provided by FSL (JHU DTI-based WM atlases for WM; Harvard-Oxford cortical/subcortical structural atlases for GM).

RESULTS

General

Data are summarized in Table I. The two patient groups were matched by GSS, type of poorer performing eyes, VF measures and RNFL thickness whereas, as expected, they differed in terms of IOP. No significant differences were found among the three study groups (NTG, POAG, and NC) in terms of age ($P = 0.95$), sex ($P = 0.22$), and WMH, both for grade ($P = 0.54$; grade 0: 70.6 vs. 58.8 vs. 69%; grade 1: 17.7 vs. 23.6 vs. 27.5%; grade 2: 11.7 vs. 17.6 vs. 3.5%; no grade 3 in either groups) and volume ($P = 0.64$; 1.1 ± 2.5 cm^3 vs. 2.4 ± 4.7 cm^3 vs. 1 ± 2.4 cm^3).

Voxelwise Differences of AC

At TBSS analysis across the whole brain, NTG patients showed, compared to NC, altered DTI measures both along and beyond the visual pathway (Table II). In particular, there was (i) lower FA (0.23 ± 0.026 vs. 0.27 ± 0.036, $P < 0.001$) in the optic tracts (OT; Fig. 1a); (ii) higher AD (1.13 ± 0.08 vs. $\pm 1.01 \pm 0.026$, $P < 0.001$) in areas related to the visual system such as the OR [mapping on the inferior fronto-occipital fascicle (IFOF) and inferior longitudinal

TABLE II. Regions of the cerebral WM tracts where NTG patients showed significant DTI abnormalities with respect to NC and POAG at TBSS analysis across the whole brain

WM regions of the visual pathways (local maxima)	Side	MNI *X*, *Y*, *Z* (mm)	Cluster size (voxel no.)	*P*-value
NTG vs NC				
FA: NTG < NC				
OT	L	−3,8,22	67	<0.001
AD: NTG>NC				
WM of LOC	R	44,–61,–9	45	0.001
	R	38,–80,–7	30	<0.001
OR (IFOF/ILF)	R	35,–75,–9	71	0.001
	L	−51,–6,–7	124	0.001
	R	24,–89,–6	50	0.001
	R	13,–80,–2	225	<0.001
WM of LG	R	26,–53,–1	91	<0.001
WM regions outside the visual pathways (local maxima)				
NTG vs. NC				
AD: NTG > NC				
WM of precuneus	R	10,–59,27	54	<0.001
SLF (frontal)	R	37,2,25	46	0.002
RD: NTG > NC				
WM of frontopercular cortex/IFG	R	45,13,11	32	0.001
WM of SPL	R	−23,−51,56	31	<0.001
NTG vs. POAG				
AD: NTG < POAG				
WM of FOC	R	21,28,–9	61	<0.001
WM of FP	R	17,52,–5	51	<0.001
WM of SFG	L	−19,10,42	31	<0.001

For each DTI measure, WM regions are ordered according to increasing *Z* values of local maxima. See text for details (including values of DTI measures) and abbreviations.

fascicle (ILF)], and the WM of lateral occipital cortex (LOC) and lingual gyrus (LG) WM (Fig. 1b,c); (ii) higher AD in regions that lie outside the visual system such as the superior longitudinal fascicle (SLF, frontal) and the WM adjacent to precuneus (Fig. 1f); (iv) higher RD (0.65 ± 0.08 vs. 0.52 ± 0.04, $P < 0.001$) in nonvisual WM adjacent to the frontal operculum cortex/inferior frontal gyrus (IFG) and superior parietal lobe (SPL; Fig. 1g,h).

NTG patients showed lower AD than POAG patients (1.07 ± 0.04 vs. 1.18 ± 0.04, $P < 0.001$) in nonvisual regions such as the WM of the frontal lobe adjacent to fronto-orbital cortex (FOC), the frontal pole (FP), and the superior frontal gyrus (SFG; Fig. 2c,d). No differences in DTI measures were found between the two patient groups along the visual pathway.

POAG showed altered DTI measures with respect to NC in several clusters. Indeed, there was (i) lower FA (0.67 ± 0.06 vs. 0.75 ± 0.03, $P < 0.001$) in the visual WM (LOC) and in the F_{maj}/splenium of the CC (sCC), midbrain WM; (ii) higher AD (1.13 ± 0.03 vs. 1.05 ± 0.04, $P < 0.001$) in the visual pathway regions such as OR (ILF/IFOF) and WM of temporo-occipital fusiform cortex (TOFC) and LOC; (iii) higher AD in various nonvisual regions including FOC WM, fornix, parahyppocampus WM, uncinate fascicle, temporal pole WM, forceps minor, SLF, frontal and temporal gyrus WM, thalamic WM, subcallosal cortex WM, corticospinal tract (CST), midbrain WM, anterior thalamic radiation (ATR); (iv) higher RD (0.51 ± 0.05 vs. 0.41 ± 0.03, $P < 0.001$) mapped on the LOC WM as well as in the F_{maj}/sCC, ATR, SLF, FP, and SFG WM and CST.

Voxelwise Differences of GM Volumes

Overall, both patient groups showed GM atrophy compared with NC (NTG vs. NC: 859 ± 120 mm^3 vs. $1{,}094 \pm 127$ mm^3, $P < 0.001$; POAG vs. NC: 409.02 ± 79.23 mm^3 vs. 509.64 ± 84.04 mm^3, $P < 0.001$). Indeed, reduced volume mapped on clusters of both the visual cortex [TOFC for NTG vs. NC (Table III, Fig. 1d); occipital pole (OP), LOC, and LG for POAG vs. NC] and beyond it [precentral gyrus and IFG for NTG vs. NC (Table III, Fig. 1i); SFG and angular gyrus for POAG vs. NC]. POAG showed lower GM volume than NTG in a cluster of the LOC (103 ± 28 vs. 134 ± 26 mm^3, $P = 0.002$; Table III, Fig. 2a).

Voxelwise Differences of FC

Across the whole study population, 12 functionally relevant RSNs were found, including default mode network, frontal executive control network (ECN, medial, and medio-lateral), right and left frontoparietal working memory network, dorsal attention network, auditory/language

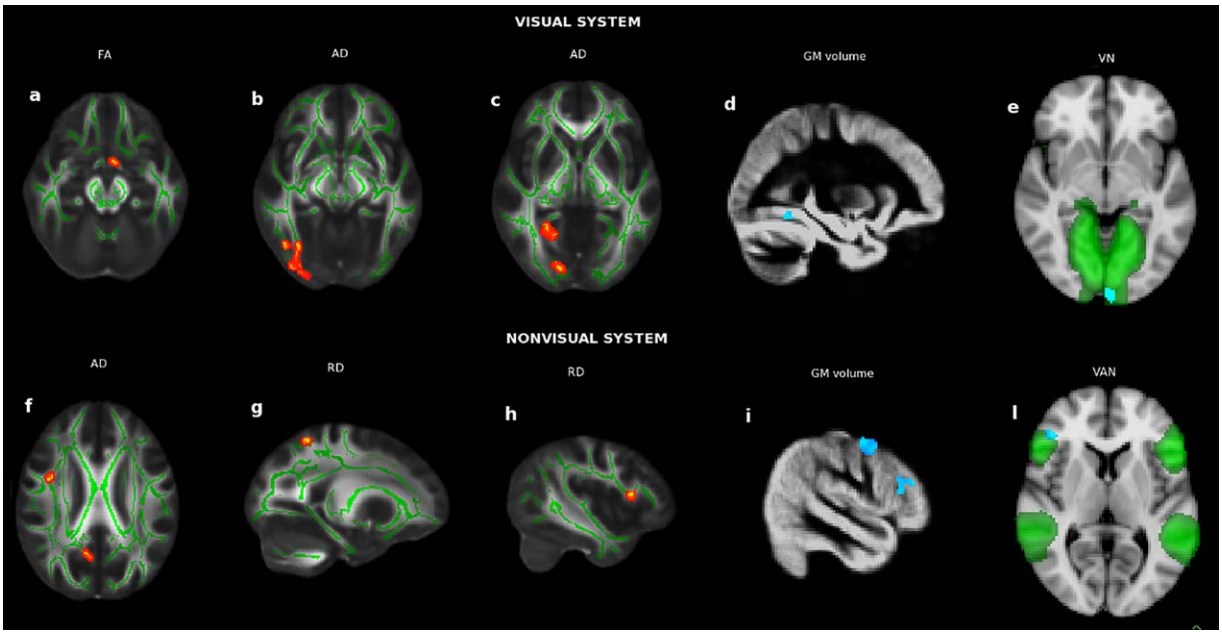

Figure 1.

Voxelwise abnormalities in NTG compared with NC at the level of visual (upper panel) and nonvisual (lower panel) system in terms of AC (a–c, f–h; in red the clusters of decreased FA, increased AD/RD; green is the WM skeleton), GM volumes (d, i; in blu-light blu the clusters of GM atrophy) and FC [e, l; in blu-light blu the clusters of changes in FC, which was decreased in VN (green) and increased in VAN (green)]. See Results section for details. [Color figure can be viewed at wileyonlinelibrary.com]

network, ventral attention network (VAN), visual networks (VN, primary, and secondary), medial temporal (limbic) network, and cerebellar network.

Compared with NC, NTG patients had lower FC in the primary VN (OP, -0.89 ± 3.29 vs. 4.13 ± 4.64, $P < 0.001$; Table IV, Fig. 1e) and higher FC in the VAN (FP/IFG, 3.42 ± 3.29 vs. -0.86 ± 3.48, $P < 0.001$; Table IV, Fig. 1l). In the comparison between NTG and POAG, the former showed lower FC in the primary VN (OP, 1.22 ± 3.04 vs. -1.53 ± 1.69, $P = 0.003$; Table IV, Fig. 2b) and medial frontal ECN (FP, 43.45 ± 54.64 vs. 0.46 ± 11.77, $P < 0.001$; Table IV, Fig. 2e). In the comparison between POAG and NC, the former showed higher FC in the medial frontal ECN (FP, 43.20 ± 55.09 vs. 8.52 ± 17.09, $P = 0.003$) and VAN (FP/IFG, 6.06 ± 5.37 vs. 0.81 ± 3.65, $P < 0.001$).

The only altered internetwork FC was present in the POAG with respect to NC, with higher partial correlation between secondary VN and limbic network [median (range): 0.037 (from −1.3 to 1.28) vs. −0.66 (from −1.78 to 1.31), $P = 0.0028$].

DISCUSSION

Damage to Visual System

In the group of NTG patients, when compared with a NC group, we found abnormalities in posterior WM regions of the visual pathway [OR (ILF/IFOF) and occipital WM (LOC, LG)] in terms of reduced FA and increased AD. Two mechanisms can explain these findings. However, there may be retrograde (Wallerian) degeneration of WM fibers along the visual pathway, as demonstrated by the reduced FA, a marker of WM tract organization and integrity, at the level of OT, which is part of the anterior visual pathway. However, due to a reduced disease-related visual input, there may be anterograde (transynaptic) degeneration, which may render some structures of the visual pathway particularly vulnerable to damage.

Interestingly, both groups of POAG and NTG patients were not significantly different in the microstructural abnormalities to visual pathway. However, there was more GM atrophy in POAG mapping on regions of both primary and secondary (association) visual cortex, whereas in NTG this was found only in the fusiform cortex, part of the secondary lateral visual cortex. Fusiform cortex is involved in high-level visual processing of color information and face recognition [Grill-Spector et al., 2004; Hubbard and Ramachandran, 2005].

In terms of FC, we found lower FC in the primary VN (OP) of NTG compared with NC. This may be secondary to disease-related visual impairment or to damage of connected WM tracts in the occipital WM, which indeed was demonstrated by the previously mentioned DTI findings. Functionally, the primary VN is involved in the early

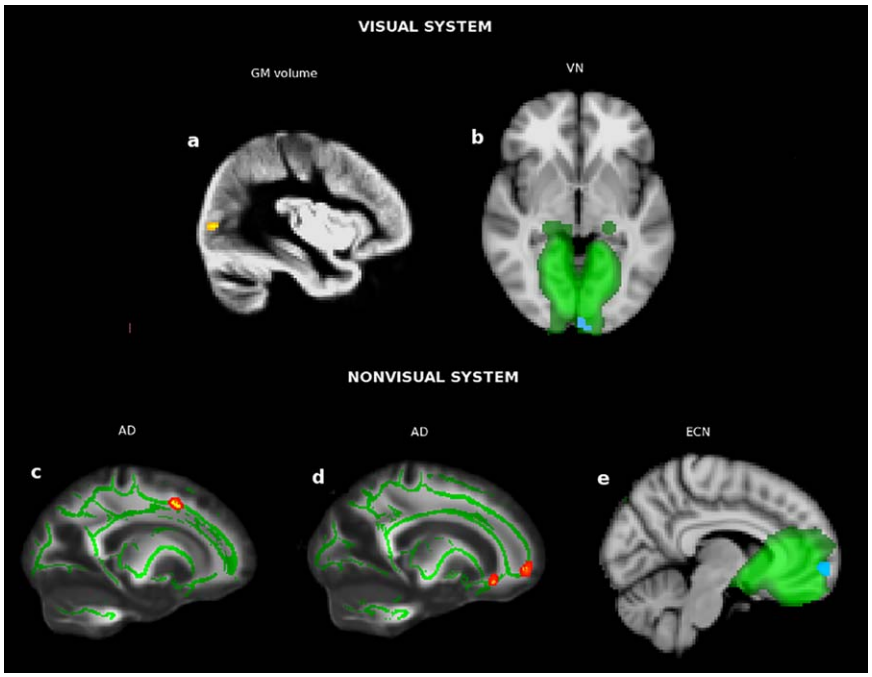

Figure 2.
Voxelwise differences between NTG and POAG at the level of visual (upper panel) and nonvisual (lower panel) system in terms of AC (c, d; in red increased AD in POAG; green is the WM skeleton), GM volumes (a; in red/yellow the cluster of increased GM volume in NTG) and FC (b, e; in blu/light blu the clusters of decreased FC in NTG within the corresponding brain networks, in green) See Results section for details. [Color figure can be viewed at wileyonlinelibrary.com]

visual processing, by receiving the visual information from the lateral geniculate nucleus and sending such information to the secondary visual cortex. The higher FC in POAG with respect to NTG, which also mapped on the OP of the primary VN may be seen as adaptive/compensatory role towards a more severe GM atrophy of the visual cortex, as above mentioned and/or to higher IOP. This finding is further supported by a higher long-range FC between secondary VN and limbic network in POAG compared with NC. Interestingly, these two networks, alongside somatosensory network, share significant similarity in terms of frequency-specific representation of cortical activity ("connectome harmonics") [Atasoy et al., 2016]. Anatomically, regions of the medial temporal lobe connect with visual association areas implicated in processing social signals such as facial actions [Freese and Amaral, 2006].

Overall, the findings suggest that even without a significant increase in IOP, NTG show brain changes across the visual system. However, the occurrence of more atrophy

TABLE III. Regions of the cerebral GM where NTG patients showed significant volume difference with respect to NC and POAG at FSL-VBM analysis across the whole brain

GM regions of the visual cortex (local maxima)	Side	MNI *X*, *Y*, *Z* (mm)	Cluster size (voxel no.)	*P*-value
Volume*: NTG < NC*				
TOFC	R	32,–54,–10	46	0.002
Volume*: NTG > POAG*				
LOC	L	−38,–80,2	34	<0.001
GM regions outside the visual cortex (local maxima)				
Volume*: NTG < NC*				
IFG	L	−46,24,14	88	0.003
Precentral gyrus	L	−44,–8,46	224	0.001

GM regions are ordered according to increasing *Z* values. See text for details (including values of GM volumes) and abbreviations.

TABLE IV. GM regions of the RSNs where NTG patients showed significant FC differences with respect to NC and POAG at probabilistic ICA across the whole brain

GM regions of the VN (local maxima)	Side	MNI *X*, *Y*, *Z* (mm)	Cluster size (voxel no.)	*P*-value
FC: NTG < NC				
VN (primary)				
OP	M	0,–98,–4	51	<0.001
FC: NTG < POAG				
VN (primary)				
OP	M	0,–100,–6	49	<0.001
GM regions outside the VN (local maxima)				
FC: NTG > NC				
VAN				
FP/IFG	R	44,36,6	34	0.001
FC: NTG < POAG				
ECN (medial frontal)	M	0,64,–2	115	<0.001
FP	M	0,64,–2	115	<0.001

Clusters in each RSN are ordered according to increasing *Z* values. See text for details (including values of FC) and abbreviations.

in the visual cortex and higher FC of the VN, both at short and long-range, in POAG with respect to NTG may reflect a possible worsening role of raised IOP.

Damage to Nonvisual System

In a recent DTI study on NTG patients from Japan, where the disease has a high prevalence, using a similar analysis (TBSS) but a different statistical approach, decreased FA was found compared to NC in the occipital WM comprising OR and F_{maj} but also in nonvisual areas such as CC and parietal lobe [Boucard et al., 2016]. Because our study on a relatively small population has an exploratory nature, we used a less conservative threshold compared with the above study. We confirmed FA alterations in similar regions but we also found more extensive damage, including altered (axial and radial) diffusivities in additional regions of both the visual and nonvisual pathways. Indeed, altered AC in NTG patients compared to NC was found in the frontal WM including the SLF frontal fibers (higher AD) and WM of fronto-opercular cortex/IFG (higher RD) and in the parietal WM of precuneous (higher AD) and SPL (higher RD). Such structures are related with higher aspects of visual and cognitive processing. Indeed, SLF provides the prefrontal cortex with information on the perception of visual space and supplies the parietal cortex (SPL, precuneous) with information on focusing spatial attention and memory retrieval of spatial information. Frontal operculum exerts cognitive control by regulating activity changes in multiple posterior occipitotemporal cortical areas for attention and appropriate response selection to memory-stored stimuli [Higo et al., 2011]. IFG on the right hemisphere plays various roles such as implementing strategies for multicomponent behavior [Dippel and Beste, 2015], constructing shape confidence for perceptual decision-making [Sherman et al., 2016] and is recruited during a particular form of executive control referred to as response inhibition [Hampshire et al., 2010]. Because all of these structures lie well outside the visual pathway, their mechanism of damage should not involve a direct degeneration spread from visual pathway but rather should reflect a primary neuropathological process. In comparison with POAG, however, AC of NTG was less altered in various frontal WM regions including FOC, FP, and SFG.

NTG brain was also characterized by unanticipated atrophy, compared with NC, in frontal cortex regions unrelated to vision and involved in language processing (left IFG) and motor control (precentral gyrus). The pattern of atrophy of NTG resembles that of aging for the involvement of the frontal cortex but it is also different from it due to the atrophy, as previously mentioned, of visual cortex, which is usually spared in aging [Grady, 2012].

Outside the VN, both NTG and POAG showed increased FC compared with NC in the VAN at the level of FP/IFG, probably due to a compensatory functional reorganization. The VAN normally exerts activity increases upon detection of behaviorally relevant targets, especially when they are salient or unexpected [Fox et al., 2006]. However, FC within the frontal ECN of POAG was higher compared with both NC, in line with our previous study on advanced POAG [Frezzotti et al., 2014], and also NTG.

Overall, mirroring the findings of the visual system, changes in nonvisual brain areas of NTG suggest their independency from the increases in IOP whereas greater AC and FC changes in nonvisual brain areas of POAG with respect to NTG supports the idea that raised IOP would be a worsening factor. In line with this, previous findings on glaucoma animal models showed IOP-sensitive increase in amyloid beta (Aβ) [Gupta et al., 2016], whose accrual and spreading occur across the Alzheimer disease brain. However, according to a novel hypothesis, a relevant role in glaucoma would be played not by IOP but rather by a dysfunction of the "glymphatic system," a brain-wide paravascular pathway for CSF and

interstitial fluid exchange, which might cause an alteration of neurotoxins, including Aβ, with reduced clearance from ON in NTG or, alternatively, an increased production in POAG [Wostyn et al., 2015]. In terms of NTG pathogenesis, it was also suggested the occurrence of high IOP spikes at night, thus being not captured during daytime measurements [Shields, 2008]. However, the lack in NTG of a continuously raised IOP, as found in POAG, should rule out it as a relevant determinant of widespread brain alterations, which turned out to be relatively similar to POAG in our study. Another putative pathogenic factor of NTG is vascular dysfunction and ischemia due to insufficient blood flow and altered vascular autoregulation [Pasquale, 2016]. This was also ruled out in our study, in view of the fact that the three study groups did not show differences in terms of WMH, which are expression of small vessel vascular changes.

Some methodological aspects are worth mentioning. In statistical terms, due to the small sample size, which did not allow enough statistical power, we used an "explorative" uncorrected voxelwise threshold of $P \leq 0.005$, cluster size ≥ 30 voxels and then, following a previous approach [Anjari et al., 2007; Frezzotti et al., 2014, 2016] we used a post-hoc Bonferroni correction, to reduce false positive rate. In terms of MRI data, both DTI and FMRI images were acquired in a reasonable scan time for patients, according to protocols extensively used on clinical MR scanners. The use of cutting-edge imaging analysis software tools (TBSS for AC, MELODIC/dual regression/FSLNets for FC) should have minimized the effects of relatively large voxel size, partial volume effect, misregistration, and relatively short scan time of resting FMRI.

In conclusion, the occurrence of brain alterations beyond those expected as a consequence of propagated ON damage provides evidence that an independent and widespread brain pathogenic process seems to occur not only in POAG, but also in NTG, with mechanisms that seem to be at least in part independent of the increases in IOP. Our findings further supports the hypothesis that glaucoma can be considered as a neurodegenerative condition, where the mechanism of neurodegeneration spreading [Hardy and Revesz, 2012] could explain the MRI findings of widespread brain structural damage and functional changes.

ACKNOWLEDGMENTS

The authors thank Riccardo Tappa Brocci (University of Siena) for help with MRI data acquisition.
The authors report no specific conflict of interest for this study

REFERENCES

Anjari M, Srinivasan L, Allsop JM, Hajnal JV, Rutherford MA, Edwards AD, Counsell SJ (2007): Diffusion tensor imaging with tract-based spatial statistics reveals local white matter abnormalities in preterm infants. Neuroimage 35:1021–1027.

Atasoy S, Donnelly I, Pearson J (2016): Human brain networks function in connectome-specific harmonic waves. Nat Commun 7:10340.

Beckmann CF, Smith SM (2004): Probabilistic independent component analysis for functional magnetic resonance imaging. IEEE Trans Med Imaging 23:137–152.

Beckmann CF, DeLuca M, Devlin JT, Smith SM (2005): Investigations into resting-state connectivity using independent component analysis. Philos Trans R Soc Lond B Biol Sci 360: 1001–1013.

Beckmann CF, Mackay CE, Filippini N, Smith SM (2009): Group comparison of resting-state FMRI data using multi-subject ICA and dual regression. Organization for Human Brain Mapping Annual Meeting. Neuroimage 47:S148.

Bonomi L, Marchini G, Marraffa M, Bernardi P, De Franco I, Perfetti S, Varotto A, Tenna V (1998): Prevalence of glaucoma and intraocular pressure distribution in a defined population. The Egna-Neumarkt Study. Ophthalmology 105:209–215.

Boucard CC, Hanekamp S, Ćurčić-Blake B, Ida M, Yoshida M, Cornelissen FW (2016): Neurodegeneration beyond the primary visual pathways in a population with a high incidence of normal-pressure glaucoma. Ophthalmic Physiol Opt 36:344–353.

Dai H, Morelli JN, Ai F, Yin D, Hu C, Xu D, Li Y (2013): Resting-state functional MRI: Functional connectivity analysis of the visual cortex in primary open-angle glaucoma patients. Hum Brain Mapp 34:2455–2463.

Dippel G, Beste C (2015): A causal role of the right inferior frontal cortex in implementing strategies for multi-component behaviour. Nat Commun 6:6587.

Douaud G, Smith S, Jenkinson M, Behrens T, Johansen-Berg H, Vickers J, James S, Voets N, Watkins K, Matthews PM, James A (2007): Anatomically related grey and white matter abnormalities in adolescent-onset schizophrenia. Brain 130:2375–2386.

Fazekas F, Chawluk JB, Alavi A, Hurtig HI, Zimmerman RA (1987): MR signal abnormalities at 1.5 T in Alzheimer's dementia and normal aging. Am J Roentgenol 149:351–356.

Fox MD, Corbetta M, Snyder AZ, Vincent JL, Raichle ME (2006): Spontaneous neuronal activity distinguishes human dorsal and ventral attention systems. Proc Natl Acad Sci U S A 103: 10046–10051.

Freese JL, Amaral DG (2006): Synaptic organization of projections from the amygdala to visual cortical areas TE and V1 in the macaque monkey. J Comp Neurol 496:655–667.

Frezzotti P, Giorgio A, Motolese I, De Leucio A, Iester M, Motolese E, Federico A, De Stefano N (2014): Structural and functional brain changes beyond visual system in patients with advanced glaucoma. PLos One 9:e105931.

Frezzotti P, Giorgio A, Toto F, De Leucio A, De Stefano N (2016): Early changes of brain connectivity in primary open angle glaucoma. Hum Brain Mapp 37:4581–4596.

Giorgio A, Stromillo ML, De Leucio A, Rossi F, Brandes I, Hakiki B, Portaccio E, Amato MP, De Stefano N (2015): Appraisal of brain connectivity in radiologically isolated syndrome by modeling imaging measures. J Neurosci 35:550–558.

Good CD, Johnsrude IS, Ashburner J, Henson RN, Friston KJ, Frackowiak RS (2001): A voxel-based morphometric study of ageing in 465 normal adult human brains. Neuroimage 14: 21–36.

Grady C (2012): The cognitive neuroscience of ageing. Nat Rev Neurosci 13:491–505.

Grill-Spector K, Knouf N, Kanwisher N (2004): The fusiform face area subserves face perception, not generic within-category identification. Nat Neurosci 7:555–562.

Gupta V, Gupta VB, Chitranshi N, Gangoda S, Vander Wall R, Abbasi M, Golzan M, Dheer Y, Shah T, Avolio A, Chung R, Martins R, Graham S (2016): One protein, multiple pathologies: Multifaceted involvement of amyloid beta in neurodegenerative disorders of the brain and retina. Cell Mol Life Sci 73: 4279–4297.

Hampshire A, Chamberlain SR, Monti MM, Duncan J, Owen AM (2010): The role of the right inferior frontal gyrus: Inhibition and attentional control. Neuroimage 50:1313–1319.

Hardy J, Revesz T (2012): The spread of neurodegenerative disease. N Engl J Med 366:2126–2128.

Higo T, Mars RB, Boorman ED, Buch ER, Rushworth MF (2011): Distributed and causal influence of frontal operculum in task control. Proc Natl Acad Sci U S A 108:4230–4235.

Hodapp E, Parrish RK, Andersson DR (1993): Clinical decision in glaucoma. St. Louis: C.V. Mosby Company.

Hubbard EM, Ramachandran VS (2005): Neurocognitive mechanisms of synesthesia. Neuron 48:509–520.

Iester M, Swindale NV, Mikelberg FS (1997): Sector-based analysis of optic nerve head shape parameters and visual field indices in healthy and glaucomatous eyes. J Glaucoma 6:370–376.

Jenkinson M, Smith S (2001): A global optimisation method for robust affine registration of brain images. Med Image Anal 5:143–156.

Jenkinson M, Beckmann CF, Behrens TE, Woolrich MW, Smith SM (2012): FSL. Neuroimage 62:782–790.

Jiang MM, Zhou Q, Liu XY, Shi CZ, Chen J, Huang XH (2017): Structural and functional brain changes in early- and mid-stage primary open-angle glaucoma using voxel-based morphometry and functional magnetic resonance imaging. Medicine (Baltimore) 96:e6139.

Klein BE, Klein R, Sponsel WE, Franke T, Cantor LB, Martone J, Menage MJ (1992): Prevalence of glaucoma. The Beaver Dam Eye Study. Ophthalmology 99:1499–1504.

Mallick J, Devi L, Malik PK, Mallick J (2016): Update on normal tension glaucoma. J Ophthalmic Vis Res 11:204–208.

Oguz I, Farzinfar M, Matsui J, Budin F, Liu Z, Gerig G, Johnson HJ, Styner M (2014): DTIPrep: Quality control of diffusion-weighted images. Front Neuroinform 8:4.

Okuda DT, Mowry EM, Beheshtian A, Waubant E, Baranzini SE, Goodin DS, Hauser SL, Pelletier D (2009): Incidental MRI anomalies suggestive of multiple sclerosis: The radiologically isolated syndrome. Neurology 72:800–805.

Pantoni L, Garcia JH (1997): Pathogenesis of leukoaraiosis: A review. Stroke 28:652–659.

Pasquale LR (2016): Vascular and autonomic dysregulation in primary open-angle glaucoma. Curr Opin Ophthalmol 27:94–101.

Polman CH, Reingold SC, Banwell B, Clanet M, Cohen JA, Filippi M, Fujihara K, Havrdova E, Hutchinson M, Kappos L, Lublin FD, Montalban X, O'Connor P, Sandberg-Wollheim M, Thompson AJ, Waubant E, Weinshenker B, Wolinsky JS (2011): Diagnostic criteria for multiple sclerosis: 2010 revisions to the McDonald criteria. Ann Neurol 69:292–302.

Pruim RH, Mennes M, van Rooij D, Llera A, Buitelaar JK, Beckmann CF (2015): ICA-AROMA: A robust ICA-based strategy for removing motion artifacts from fMRI data. Neuroimage 112:267–277.

Schoemann J, Engelhorn T, Waerntges S, Doerfler A, El-Rafei A, Michelson G (2014): Cerebral microinfarcts in primary open-angle glaucoma correlated with DTI-derived integrity of optic radiation. Invest Ophthalmol Vis Sci 55:7241–7247.

Sherman MT, Seth AK, Kanai R (2016): Predictions shape confidence in right inferior frontal gyrus. J Neurosci 36:10323–10336.

Shields MB (2008): Normal-tension glaucoma: Is it different from primary open-angle glaucoma? Curr Opin Ophthalmol 19: 85–88.

Shiose Y, Kitazawa Y, Tsukahara S, Akamatsu T, Mizokami K, Futa R, Katsushima H, Kosaki H (1991): Epidemiology of glaucoma in Japan–a nationwide glaucoma survey. Jpn J Ophthalmol 35:133–155.

Smith SM, Jenkinson M, Woolrich MW, Beckmann CF, Behrens TE, Johansen-Berg H, Bannister PR, De Luca M, Drobnjak I, Flitney DE, Niazy RK, Saunders J, Vickers J, Zhang Y, De Stefano N, Brady JM, Matthews PM (2004): Advances in functional and structural MR image analysis and implementation as FSL. Neuroimage 23:S208–S219.

Smith SM, Fox PT, Miller KL, Glahn DC, Fox PM, Mackay CE, Filippini N, Watkins KE, Toro R, Laird AR, Beckmann CF (2009): Correspondence of the brain's functional architecture during activation and rest. Proc Natl Acad Sci U S A 106: 13040–13045.

Van Herick W, Shaffer RN, Schwartz A (1969): Estimation of width of angle of anterior chamber. Incidence and significance of the narrow angle. Am J Ophthalmol 68:626–629.

Wang J, Li T, Sabel BA, Chen Z, Wen H, Li J, Xie X, Yang D, Chen W, Wang N, Xian J, He H (2016): Structural brain alterations in primary open angle glaucoma: A 3T MRI study. Sci Rep 6:18969.

Wang J, Li T, Wang N, Xian J, He H (2017): Graph theoretical analysis reveals the reorganization of the brain network pattern in primary open angle glaucoma patients. Eur Radiol 26: 3957–3967.

Winkler AM, Ridgway GR, Webster MA, Smith SM, Nichols TE (2014): Permutation inference for the general linear model. Neuroimage 92:381–397.

Wostyn P, Van Dam D, Audenaert K, Killer HE, De Deyn PP, De Groot V (2015): A new glaucoma hypothesis: A role of glymphatic system dysfunction. Fluids Barriers CNS 12:16.

Zhang YQ, Li J, Xu L, Zhang L, Wang ZC, Yang H, Chen CX, Wu XS, Jonas JB (2012): Anterior visual pathway assessment by magnetic resonance imaging in normal-pressure glaucoma. Acta Ophthalmol 90:e295–e302.

Zikou AK, Kitsos G, Tzarouchi LC, Astrakas L, Alexiou GA, Argyropoulou MI (2012): Voxel-based morphometry and diffusion tensor imaging of the optic pathway in primary open-angle glaucoma: A preliminary study. Am J Neuroradiol 33: 128–134.